

AMF-Placer 2.0: Open Source Timing-driven Analytical Mixed-size Placer for Large-scale Heterogeneous FPGA

Tingyuan Liang*, Gengjie Chen[†], Jieru Zhao[‡], Sharad Sinha[§] and Wei Zhang*

*ECE Department, Hong Kong University of Science and Technology;

[†]CSE Department, Chinese University of Hong Kong

[‡]CSE Department, Shanghai Jiao Tong University; [§]CSE Department, Indian Institute of Technology Goa

tliang@connect.ust.hk, gjchen@cse.cuhk.edu.hk, zhao-jieru@sjtu.edu.cn, sharad@iitgoa.ac.in, eeweiz@ust.hk

Abstract—To enable the performance optimization of application mapping on modern field-programmable gate arrays (FPGAs), certain critical path portions of the designs might be prearranged into many multi-cell macros during synthesis. These movable macros with constraints of shape and resources lead to challenging mixed-size placement for FPGA designs which cannot be addressed by previous analytical placers. Moreover, general timing-driven placement algorithms are facing challenges when handling real-world application design and ultrascale FPGA architectures. In this work, we propose AMF-Placer 2.0, an open-source comprehensive timing-driven Analytical Mixed-size FPGA placer. It supports mixed-size placement of heterogeneous resources (e.g., LUT/FF/LUTRAM/MUX/CARRY/DSP/BRAM) on FPGA, with an interface to Xilinx Vivado. To speed up the convergence and improve the timing quality of the placement, standing upon the shoulders of AMF-Placer 1.0, AMF-Placer 2.0 is equipped with a series of new techniques for timing optimization, including a simple but effective timing model, placement-blockage-aware anchor insertion, WNS-aware timing-driven quadratic placement, and sector-guided detailed placement. Based on a set of the latest large open-source benchmarks from various domains for Xilinx Ultrascale FPGAs, experimental results indicate that critical path delays realized by AMF-Placer 2.0 are averagely 2.2% and 0.59% higher than those achieved by commercial tool Xilinx Vivado 2020.2 and 2021.2 respectively. Meanwhile, the average runtime of placement procedure of AMF-Placer 2.0 is 14% and 8.5% higher than Xilinx Vivado 2020.2 and 2021.2 respectively. Although limited by the absence of the exact timing model of the device, the information of design hierarchy and accurate routing feedback, AMF-Placer 2.0 is the first open-source FPGA placer which can handle the timing-driven mixed-size placement of practical complex designs with various FPGA resources and achieves the comparable quality to the latest commercial tools.

Index Terms—timing-driven placement, analytical placement, mixed-size placement, FPGA

I. INTRODUCTION

Field-programmable gate array (FPGA) is an integrated circuit designed to be reconfigured by users after manufacturing. As shown in the example in Fig. 1, the latest island-style FPGA, which is columnar and heterogeneous, contains a 2D array of configurable sites, each of which consists of basic elements of logic (BELs) [1]. For example, configurable logic block (CLB) sites consist of BELs like look-up tables (LUTs), flip-flops (FFs), multiplexers (MUXs) and carry chains (CARRYs). Some other sites contain larger heterogeneous BELs,

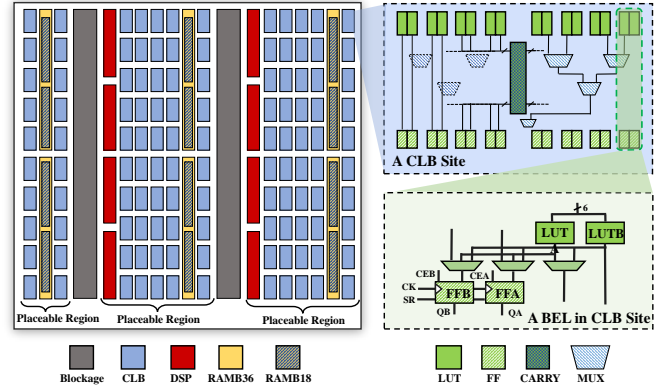


Fig. 1. Example of Xilinx Ultrascale FPGA device, a CLB site, and a BEL in it

e.g. digital signal processors (DSPs) and block random access memories (BRAMs).

During FPGA placement, the netlist generated by logic synthesis should be placed on discrete sites on the FPGA device, with the goal of shorter routing wirelength, less congestion regions and better timing, under the constraints of the device architecture. Typically, this placement flow includes the following steps: (1) initial placement/floorplanning to generate a very rough placement; (2) global placement to find optimal locations for the elements to optimize wirelength and timing under the resource constraints; (3) packing and legalization to exactly map each element to valid FPGA site; (4) detailed placement to resolve the worst cases locally and optimize the metrics.

With advancement in semiconductor, FPGAs have increased in size as well as the variety of resources available on them and the overall architecture. Meanwhile, FPGA applications become much more complex and denser. These factors bring many new challenges to the placement flow.

Due to the upstream optimization, macros with constraints of shape and resource [2] [3] might be generated, like the examples shown in Fig. 2. In this paper, we use **standard cell** to denote the smallest, indivisible, representable instance in the design netlist and use **macro** to denote a fixed group of multiple standard cells with constraints of their relative locations. For example: (1) 1 MUX and 2 LUTs connected to it

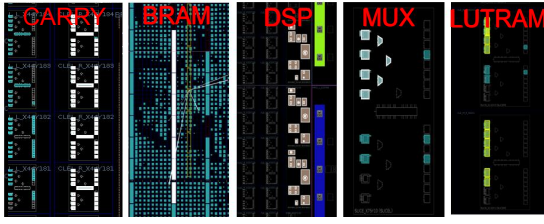


Fig. 2. Example of various types of macros with shape constraints: the macros are highlighted.

should be treated as a macro; (2) a BRAM, without cascading with other BRAMs, is a standard cell; (3) 3 cascaded DSPs should be regarded as a macro. On the FPGA device, a macro might require multiple BELs spanning sites. Moreover, macros will lead to high interconnection density. These common scenarios in modern FPGA designs are seldom considered in previous exploration of FPGA placement.

A. Related Works

Some FPGA placers [4] [5], e.g., VTR, are based on simulated annealing (SA), which might lead to long synthesis time when the input netlist is large. Thus, analytical solutions using numerical approaches were proposed to solve the placement with high scalability and quality [6]. Gort and Anderson [6] presented an analytical FPGA placer HeAP, which demonstrated a $7.4\times$ runtime advantage with 6% better placement quality compared to the SA placement algorithm of VPR 5.0. Chen et al. [7] proposed analytical placement solution with efficient and effective packing achieves 50% shorter wirelength, with an $18.30\times$ overall speedup compared to VPR 7.0. During ISPD 2015/2016 contest, a series of analytical placers, e.g., UTPlaceF [8], RippleFPGA [9], GPlace [10] and NTUfplace [11], were inspired with the consideration of congestion and clock constraints and they showed promising performance on the contest benchmarks. Later in 2017, LIQUID [12] was proposed with analytical solution based on gradient-guided algorithm while elfPlace [13] cast the placement density cost to the potential energy of an electrostatic system which tried to include various cost metrics in one nonlinear model to be optimized. However, in the synthetic benchmark ISPD 2016/2017 [14] [15], the randomly-generated netlists consist of impractical interconnections e.g., each of the 36Kb Block-RAMs has only 6 input nets and 1 output nets, and there are many registers which are unnecessarily duplicated without consideration of timing and fanout, and have no design hierarchy, leading to relatively even distribution of timing criticality in the netlist. What's worse, there is no widely-used instance like CARRY, MUX, LUTRAM and 18Kb Block-RAM.

Timing-driven FPGA placement is critical for the final timing quality of an FPGA design implementation. However, timing-driven placement is hard since the mutual impact among routing wirelength, routability, and timing quality is complicated. Improper emphasis or neglect of the reduction of estimated wirelength, e.g., half perimeter wire length (HPWL), can lead to routing failure, longer routing wirelength, and worse timing [16] [17]. There are some existing

analytical solutions while the timing-driven solutions [16], [18]–[25] to ASIC placement did not consider the discrete heterogeneous resource constraints of FPGAs. Chen and Chang [26] proposed a routing-architecture-aware analytical placement to improve timing quality of FPGA implementation. Dhar et al. [27] introduced an effective detailed placement based on shortest path algorithm which was adopted by many solutions. Lin et al. [28], [29] proposed efficient delay model and timing-driven placement considering clock constraints. Nikolić et al. [30] proposed an efficient ILP-based detailed placer which moves a carefully selected subset of LUTs to efficiently improve timing.

Timing-driven placement will become more difficult when we want to handle real-world application and complex FPGA devices with many architecture constraints, like placement blockages, packing legalization, clock legalization and fixed macro shapes. The existing challenges will be discussed in Section I-B.

B. Motivation

1) *Challenges of FPGA Mixed-Size Placement:* Most of previous FPGA analytical placers except HeAP [6] targeted at benchmarks which consist of only standard cells, each of which will only occupy one BEL on FPGA device, e.g., the randomly generated benchmarks in ISPD 2015/2016 contest [14] [31]. Moreover, most of them did not consider designs with commonly-used elements like MUX, CARRY, and LUTRAM [32]. The aforementioned macros with shape constraints are not considered by existing FPGA analytical placers except AMF-Placer 1.0 [33], which we have proposed to handle the following challenges in wirelength optimization, cell spreading, packing and legalization during placement:

- Some macros in FPGA design could share CLBs with other instances at fine-grained level. It means that the macros and standard cells can "overlap" to some extents in FPGA mixed-size placement.
- Legalization in previous works on FPGA analytical placement are 1-to-1 legalization, i.e., one instance will require only one site. However, in mixed-size placement, the legalization of macros might be 1-to-many, i.e., one instance might require multiple sites.
- Latest designs might include a large number of macros. For example, in Minimap2 [34], there are 8782 macros and 499104 standard cells. Existing cell spreading algorithms for FPGA might fail to efficiently resolve resource overflow caused by a large number of macros.

2) *Challenges of FPGA Timing-driven Placement:* Various timing-driven FPGA placers have been developed, but a comprehensive practical placement flow is still challenging from a wide range of perspectives:

- Timing-driven FPGA placer relied on corresponding analytical models [26], [28], [29] to link the timing metrics to the analytical optimization problem. However, directly integrating these analytical timing models into the optimization objective functions does not guarantee that the final placement will converge at optimal timing results,

since there are numerous local optima in the nonconvex objective functions.

- Global placement algorithms in previous works, which are only guided by TNS (total negative slacks), neglecting the impact of WNS (worst negative slack), might downgrade the final WNS results.
- Latest detailed placement algorithms are commonly based on shortest path algorithm [27], suffering low-efficiency identification of candidate locations for involved instances and a lack of fast evaluation of global impact after the optimization of a specific path.
- The complexity of application netlist and FPGA architectures has been raised dramatically. For example, the target devices and design of [26], [28], [29] were relatively simpler and smaller compared to the latest ultrascale FPGA device so a comprehensive solution considering complex FPGA architecture factors (e.g., placement blockage, control set constraints and CLB packing) and large designs with complicated hierarchy is absent.

3) *Impact of Macro Instances on Timing Optimization* : Specially, mixed-size instances make timing optimization further difficult due to the following factors:

- Compared to standard cells, macros have many more pins and nets connected with other instances. For example, a CARRY macro could connect to more than 200 nets outside the macro. A large number of macros with high fanin and high fanout in the circuit netlist will lead to numerous intersection in the critical timing paths, which makes timing optimization for these critical path challenging. For example, moving one instance for timing optimization of one timing path might lead to serious timing downgrading of many other timing paths.
- The large macros can easily disturb the placement of the other instances on some critical timing paths even if the macros are not parts of the timing paths, since macros demand multiple sites or BELs. For example, a CARRY macro, which might consists of multiple cells, could occupy more than 128 BELs and 8 CLB sites, leading to the resource conflict with many other instances.

C. Contributions

AMF-Placer 1.0 [33] enables efficient mixed-size FPGA placement with parallelized techniques including: (1) simulated-annealing-based floorplanning; (2) quadratic placement with interconnection-density-aware pseudo nets and legalization-oriented anchors; (3) cell spreading algorithm with utilization-guided search window and deadlock-free area supply control; (4) and progressive macro legalization. With the consideration of the practical demands of timing quality and the scenarios in real applications with complex hierarchy where there are elements with shape constraints, standing upon the shoulders of AMF-Placer 1.0, AMF-Placer 2.0 provides the extra important features as follows:

- a set of timing optimization algorithms without involving static timing analysis (STA), e.g., path-length-aware SA-based floorplanning and parallelized CLB packing with timing factors considered.

- an efficient piecewise regression model of pin-to-pin delay, utilized by our integrated light-weight parallelized timing analysis engine.
- a placement-blockage-aware optimization scheme, which identifies the potential negative interference of placement blockage with long paths, spreads the instances in specific regions, and inserts placement anchors for the instances on the target paths to reduce cross-blockage routing.
- a WNS-aware timing-driven global placement, based on quadratic programming and proper utilization of pseudo-net with slack-guided weights, which realizes the multi-objective optimization of WNS, TNS and wirelength.
- a sector-guided detailed placement algorithm, which can efficiently identify the instance movement with promising timing benefits and simultaneously optimize WNS and TNS. The timing can be comprehensively optimized by AMF-Placer 2.0 at various granularity levels (i.e., multi-path, per-path, and per-instance).

The source code and Wiki of our proposed AMF-Placer 2.0 and involved open-source benchmarks are available at <https://github.com/zslwyuan/AMF-Placer>.

II. PRELIMINARIES

In this section, we describe the mixed-size placement problem in FPGA scenarios and our analytical placement framework.

A. FPGA Macro Characteristics

As per examples shown in Fig.2, the standard cells in a macro must be placed in adjacent sites in the same column according to the downstream flow requirements. Usually, each macro could include one type of core cells, which could be CARRY cells, MUX cells, LUTRAM cells, DSP cells, or BRAM cells. Apart from the core cells, a macro might also include some peripheral LUT/FF cells, which are directly connected to the core cells. According to the core cell type, the macros can be mainly classified into 5 types and their major characteristics are listed as below:

- The CARRYs connected with carry in/out port should be extracted as a macro and moreover, the LUTs and FFs connected to the related CARRYs should be assigned in the same macro. Furthermore, to enable the routing of some input pins of CARRY, which connect to signals outside the CLB site, some corresponding LUT slots in the same CLB site should be transformed into non-logic route-thru LUTs, which are not in the original netlist. Similarly, FF slots in CLBs might be unavailable due to routing resource contention in CARRY macros.
- A MUX with its two input standard cells, which could be two LUTs or two other MUXes, should be extracted as a macro. MUX macros will also lead to route-thru usage of LUTs or disable external interconnection of some FFs because of the routing of selection signals.
- LUTRAM standard cells, which share input net for read/write address and data bits, should be extracted as a macro. This kind of macros have to be located in SLICEM columns of the device.

- For DSPs and RAMs, they might be cascaded to handle larger demand of computation and storage. The standard cells in one of these macros are interconnected by the nets of their cascaded input/output signals. Please note that for each RAMB36E2 standard cell, we will consider it as a macro with 2 RAMB18E2 for legalization.

AMF-Placer 2.0 inherit the ability of AMF-Placer 1.0 [33] to detects the macros in design netlist and generates placeholders to occupy resources and meet internal routing constraints. There are some other minor macros defined by vendor primitives [3], which are out of the scope of this work. More details are available in the device documentations [35]–[37].

B. Problem Formulation

The placement of the instances in a FPGA-based design can be formulated as a hypergraph $H = (V, E)$ placement problem. Let vertices $V = \{v_1, v_2, \dots, v_n\}$ represent n instances in the design netlist and hyperedges $E = \{e_1, e_2, \dots, e_m\}$ represent m nets. Let x_i and y_i be the x and y coordinates of the center of the instance v_i during placement, respectively. As mentioned in Section I, the instances can be categorized into two types, i.e., standard cells and macros, and both of these two types could be movable or fixed according to the design constraints. One of the most common objective functions for placement is the sum of half-perimeter wirelength (HPWL) over all nets, i.e., the defined E . By properly inserting weighted pin-to-pin pseudo nets, AMF-Placer 2.0 can integrate the timing objective into the conventional wirelength-driven placer. The FPGA mixed-size placer should determine the position of each movable instance (i.e., x_i and y_i) so that the objective function consisting of wirelength term and timing term is minimized under the technology and region constraints.

C. The Framework of AMF-Placer 2.0

AMF-Placer 2.0 is a comprehensive FPGA placement framework as shown in Fig. 3. The input of AMF-Placer is the pre-implementation netlist extracted from Xilinx Vivado and the output is the location of each instance on the specific device and Tcl script for Vivado to consume the generated placement. The proposed placement flow consists of STA-independent phases and STA-dependent phases.

1) STA-independent Phases:

At the early stage of placement, since instances can be moved in a wide range, it is hard to get the stable and accurate timing evaluation of the placement. Therefore, STA-independent phases, inherited from AMF-Placer 1.0 with modifications for early-stage timing optimization without involving static timing analysis, will dominate the placement optimization iterations to minimize HPWL and pave the way for timing-driven phases. These STA-independent phases includes:

(1.1) *Initial Floorplanning*: AMF-Placer starts from the initial floorplanning of the instance clusters via the connectivity-based partitioning and simulated-annealing (SA) placement. Before the partitioning, instances on timing-risky paths will be clustered. During SA placement, the blockages between

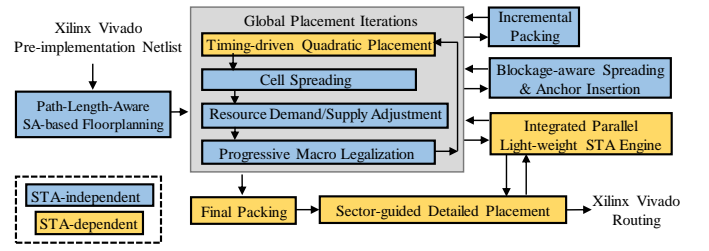


Fig. 3. The workflow of AMF-Placer 2.0 consisting STA-independent phases and STA-dependent phases

placed clusters will be considered during placement quality evaluation.

(1.2) *Blockage-aware Spreading and Anchor Insertion*: By analyzing the connectivity, timing criticality of the circuits, and the location distribution of the critical paths on the device, some instances will be clustered and anchors will be inserted for these instances to reduce the long cross-placement-blockage routing. To enable the coarse-grained movements of the clusters, instances in specific regions will be spread.

(1.3) *Cell Spreading Based on the area demand of instances and the area supply of the devices*, instances will be spread from the regions where demand for resources is outrunning supply, to other regions. Techniques are involved to avoid spreading deadlock and unnecessary aggressive displacement. The spreading region for each cell is determined by both resource utilization and placement blockage for timing benefits.

(1.4) *Resource Demand/Supply Adjustment*: Based on the packing feasibility and routing congestion level, the area demand of some standard cells like LUTs and FFs will shrink or increase and the area supply of some regions will be increased or reduced, to improve the placement quality. This phase is adopted from extended UTPlaceF [38].

(1.5) *Progressive Macro Legalization*: Each macro will be mapped to multiple potential locations or one exact location according to the confidence. Moreover, anchors will be set to those locations for the macro and pseudo nets will be inserted between the macro and the anchors to facilitate the convergence.

(1.6) *Incremental Packing*: During the global placement, some LUTs and FFs will be paired as LUT-FF macros and FF-FF macros to shrink the problem size and improve the placement quality by identifying CLB internal nets at early stage. This phase is adopted from RippleFPGA [9].

2) STA-dependent Phases:

When the wirelength tends to be stable, timing-driven phases will further optimize the timing quality of the placement based on static timing analysis. These timing-driven phases includes:

(2.1) *Timing Model and Timing Analysis*: Based on the dataset of timing delays, we use a piece-wise function based on non-integer polynomials to fit the distribution of timing delays with various differences of the X-Y coordinates of interconnected pins on FPGA. Based on this regression model of timing and the ideas of OpenTimer [39], a light-weight parallel static timing analysis engine is implemented.

(2.1) *Timing-driven Quadratic Placement*: For each in-

stance, its next location will be determined by solving a quadratic optimization problem related to wirelength and timing. To handle mixed-size placement, interconnection density and legalization are considered in quadratic placement with proposed adaptive pseudo net weights and pseudo nets for legalization. Moreover, timing-oriented pseudo nets will be inserted between pins and the strength of these pseudo nets will be determined based on both local timing slack of related paths and global timing quality.

(2.2) *Global Packing*: After the global placement iterations, each instance will be mapped to sites, each of which consists of fixed number and types of resource, as exact legalization. For example, LUTs, FFs, MUXs and CARRYs should be mapped to CLB. In this phase, clock legalization constraints should be handled carefully, CLB internal interconnection should be maximized and timing factor should be involved.

(2.3) *Detailed Placement*: Global placement and global packing evaluate the quality of placement from the global perspectives, while detailed placement will handle those local critical paths play little roles in the global evaluation objectives at the granularity level of multi-path, per-path, and per-instance.

Most of the related algorithms for these phases are parallelized. Detailed methodologies will be illustrated in the following section III and IV.

III. IMPLEMENTATION OF STA-INDEPENDENT PHASES

In this section, we will illustrate the implementation of STA-independent phases which do not rely on static timing analysis (STA). Some STA-independent phases are based on AMF-Placer 1.0, and we will focus on the illustration of the additional important timing-oriented modifications.

A. Initial Floorplanning

Compared to the randomly generated FPGA netlists [14] [31] or small designs [6], large-scale real-world designs from various domains, like those shown in Section V, usually feature specific architecture and hierarchies. Moreover, on FPGA, the resources are separated into discrete regions and the resource supply for each type of resource is not even on the overall device. These factors of design and device make the initial floorplan have a critical aftereffect for the later timing optimization, especially considering the large macros with high fanin/fanout.

AMF-Placer 1.0 first recursively partitions the input netlist into clusters with constraints of clock and resource, based on PaToH [40], and then conducts SA-based cluster-level floorplanning before global placement iterations.

The connectivity-based partitioning/clustering algorithms used by AMF-Placer 1.0 [33] and other previous works [9] [41] do not consider timing factors in partitioning. For timing optimization, one potential approach is to assign weights to the nets based on timing slack but it might be impractical because: (1) the timing slack evaluation at the very beginning of placement is not reliable; (2) partitioning of weighted hypergraph is much slower when processing large hypergraphs [42]; (3) min-cut-oriented partitioning mainly

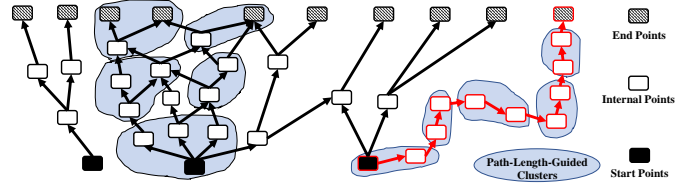


Fig. 4. Examples of clustering guided by path length with $Thr_{Dmax} = 4$

minimizes total negative slack (TNS), while due to random factors, a small number of instances on the critical paths spreading across many clusters can undermine the worst negative slack (WNS).

To realize a timing-friendly partitioning, AMF-Placer 2.0 introduces initial clustering based on timing path length, which is defined as the number of instances on the timing path. By breadth-first search (BFS) from the start points and end points of timing paths, for each instance in the netlist, we can easily obtain $D_{forward_{vi}}$ and $D_{backward_{vi}}$, which are the distance to the farthest start point among the paths including instance v_i , and the distance to the farthest end point among the paths including v_i . Accordingly, we can get $D_{max_{vi}}$, the maximum length of the paths including v_i , by summing $D_{forward_{vi}}$ and $D_{backward_{vi}}$. AMF-Placer 2.0 will sort the instances according to $D_{max_{vi}}$ in descending order first and then by $D_{forward_{vi}}$ in ascending order, and generate a corresponding sorted list of instance L_{len} . Since we are only interested in the instances on the longest paths, a path length threshold Thr_{Dmax} is introduced to select the top-5% instances in L_{len} .

AMF-Placer 2.0 will iterate the instances with $D_{max_{vi}}$ greater than Thr_{Dmax} in L_{len} . In this procedure, each instance that has not been clustered will be clustered with its unclustered direct fanout instances, as shown in Fig 4. The generated clusters will be regarded as entities during partitioning. Such fanout-based initial clustering can effectively reduce the cross-cluster interconnections in the critical paths in the final partitioning. The reasons we don't adopt the scheme of directly clustering a long path are: (1) an instance, especially for macros, might be included by multiple paths with similar lengths and deterministic clustering of a path might undermine the timing of the other paths; (2) A extremely long path could still span in a wide range in the final region, for which an example path is highlighted in red in Fig 4. Directly clustering an entire long path could be too aggressive and lead to serious limitations for later optimization.

During SA placement, the blockages between placed clusters will be considered during placement quality evaluation by adding extra cost for nets spanning across the blockages.

B. Blockage-aware Spreading and Anchor Insertion

As shown in Fig. 1, in modern FPGA devices, there are placement blockages separating a device into several available placement regions, which might be introduced by IO banks (e.g., GPIOs and PCIe interfaces) or die boundaries. The delays of nets across the blockage region will be relatively higher than the delays of the nets routed within general placement region. Most of existing works ignored this problem

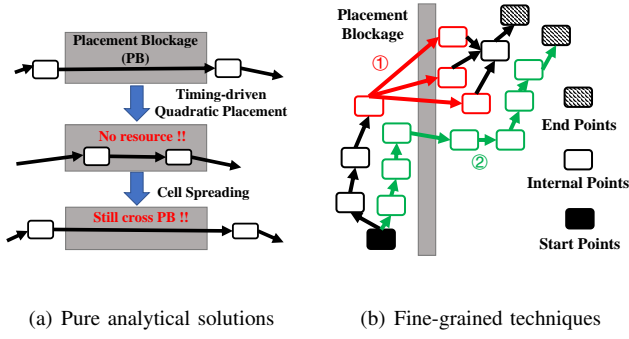


Fig. 5. Drawbacks of the other timing optimization solutions for the columnar blockage regions

during global placement since they focused on wirelength-driven placement but this problem is critical in timing-driven placement. For example, the placement blockages of PCIe interfaces are completely omitted in the device information of the benchmark ISPD 2016/2017 [14] [15].

However, as an example shown in Fig. 5(a), this problem cannot be solved by simple timing-slack-based net weights, since the reduced distance between instances across the placement blockage will be canceled by cell spreading or final packing. Furthermore, this problem cannot be solved by fine-grained local placement optimization because: (1) one net spanning the blockages might drive multiple sink instances, so while resolving the problem of one sink instance, the cross-blockage problem of the other sink instances will remain (e.g., ① in Fig. 5(b)); (2) one net might belong to a long path so while resolving the problem of a pair of instances on a path, the cross-blockage problem of the other instances on the path could be introduced (e.g., ② in Fig. 5(b)).

Therefore, we propose a coarse-grained solution to the blockage-related problem which will be involved periodically during global placement, as shown in Fig. 3.

The first step is to cluster the circuits which might contain critical paths. AMF-Placer 2.0 will iterate the instances in the sorted list L_{len} , which belong to a set $S_{crit} = \{v_i | Dmax_{v_i} > Thr_{Dmax}, Dforward_{v_i} > 0\}$. For a target instance under processing, if it is unclustered, its unclustered direct/indirect successors in S_{crit} will be traversed in the depth-first search (DFS) order of H and inserted into a cluster S_{C_j} , until the number of instances in the cluster is greater than N_C , which is set to 20000 empirically. In this step, a set of clusters will be obtained and v_i only belongs to one extracted cluster. The condition $Dforward_{v_i} > 0$ is used to constrain the depth of DFS by cutting the netlist at the timing start/end points and the reason of the depth constraint has been explained in Section III-A.

The second step is to select the target available placement region for each cluster S_{C_j} . If the proportion of the instances belonging to S_{C_j} in a specific available placement region R_{target_j} is greater than 50%, R_{target_j} will be selected as the target region for the instances in S_{C_j} . Otherwise, S_{C_j} will not be assigned to any available placement region, since it might tend to span evenly in multiple available placement regions.

The third step is to guide the movement of the instances

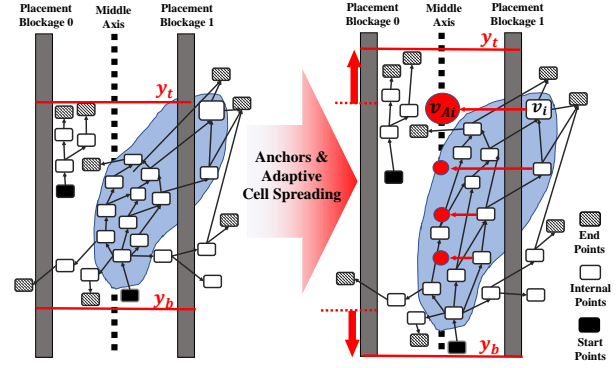


Fig. 6. Examples of Blockage-aware Spreading and Anchor Insertion: some of the pseudo nets are omitted for better visualization.

in S_{C_j} and R_{target_j} in later placement iterations. Since the available placement regions and blockages are columnar and aligned in horizontal direction for Ultrascale FPGA devices, each instances v_i in S_{C_j} will be connected to a corresponding anchor v_{Ai} at the horizontal center of R_{target_j} with the same vertical coordinate as v_i , as the example shown in Fig. 6. For the timing-driven quadratic placement which will be illustrated in Section IV-B, the weight of the pseudo net $e_b(v_i)$ connecting v_{Ai} and v_i can be formulated as:

$$w_{e_b}(v_i) = \beta \times |(x_i - x_{Ai})| \times \text{pinNum}(v_i) \quad (1)$$

where β is a constant hyperparameter and $\text{pinNum}(v_i)$ is the number of the pins of v_i . For all the instances assigned to specific target regions, their blockage-aware pseudo nets will be recorded in a set $E_b = \{e_b(v_i)\}$. According to Eqn.(1), when v_i is far from v_{Ai} , the corresponding net will be strengthened and even for v_i in their R_{target_j} , pseudo nets with lower weights will be still attached.

However, since an available placement region R_{target} could have been highly utilized or congested during placement, we need to spread the instances in it to spare area for the incoming instances, i.e., we need to stretch the existing placement in R_{target} . Let $N_{outside}$ be the number of instances will be guided to R_{target} but not in it, N_{inside} be the total number of instances in R_{target} which are not guided to the other regions, y_t be the vertical coordinate of the top instances v_t in R_{target} and y_b be the vertical coordinate of the bottom instance v_b in R_{target} . We can get a stretch ratio $\Delta r_{stretch} = N_{outside}/N_{inside}$, and the linear transformed vertical coordinates for v_t and v_b will be

$$y'_t = y_t + \Delta r_{stretch} \times (y_t - y_b)/2 \quad (2)$$

$$y'_b = y_b - \Delta r_{stretch} \times (y_t - y_b)/2 \quad (3)$$

The instances in R_{target} with original vertical coordinate between y_t and y_b will be mapped to new locations in a similar way of linear transformation of coordinate, as the example shown in Fig. 6. If y'_t or y'_b is outside the boundary of the FPGA device, it will be slightly adjusted accordingly. With the inserted anchors and specific instance spreading, the clusters with long paths across the blockages will be gradually consumed by their corresponding placement regions.

C. Cell Spreading

The fundamental cell spreading algorithm of AMF-Placer is based on widely adopted bi-partitioning rough legalization [4] [6] [9] [12] [43] [44]. During cell spreading, the FPGA device will be evenly divided into a grid of $N_Y \times N_X$ bins $B = \{B_{ij}\}$. The placer will find an overflowed bin, expand it into a corresponding larger window containing it, recursively partition the window, and spread the instances into bins in the window.

AMF-Placer 1.0 [33] has realized parallelized cell spreading algorithm by extracting non-overlap cell spreading windows. Moreover, as mentioned in Section II-A, macros might require high density of resource, span multiple sites and share CLB sites with standard cells, AMF-Placer 1.0 provided new methods to handle such mixed-size spreading, including: (1) injecting resource supply fluctuation to resolve deadlocks of macro-related cell spreading; (2) resource-utilization-guided expanding of cell spreading windows for overflow regions; and (3) forgetting-rate-based location update scheme to depress aggressive cell spreading in conventional solutions.

In AMF-Placer 2.0, we mainly include cell spreading fences for the clusters identified in Section III-B to enforce the spread instances placed within the target placement regions when the resource utilization of the regions are not overflowed.

D. Progressive Macro Legalization

As discussed in Section I-B1, 1-to-1 legalization cannot handle macro legalization. To solve this challenge of mixed-size FPGA placement, we developed parallelized progressive macro legalization for the 1-to-many legalization of a large number of macros in AMF-Placer 1.0. It will only conduct rough legalization in the early iterations of global placement, and it will involve exact legalization following rough legalization when the macros are close enough to their potential legal positions.

During rough legalization, min-cost bipartite matching, which is parallelized by extracting independent subgraphs in bipartite graph, will be used to map each standard cell in a macro to an FPGA site and standard cells in a macro are allowed to be mapped to different columns. During quadratic placement, with pseudo nets, each macro could be connected to multiple legalization anchors indicated by the rough legalization result of the standard cells belonging to it. Compared to the direct legalization [8] or cell spreading [9] for macros, AMF-Placer 1.0's solution [33] gradually strengthens the weights of the legalization pseudo nets, smoothly legalizes the large macros, and preserves space for wirelength optimization.

During exact legalization, the cell-spreading-based approach [9] is utilized to map the macros to the columns, which provide resources of the corresponding type. For intra-column legalization of AMF-Placer 1.0 [33], suppose there are $N_{macro,col}$ macros assigned to the column and $N_{site,col}$ sites in a specific column. For macros assigned in the column, they will be sorted according to their y-coordinates. Then they will be assigned indices, $0, \dots, N_{macro,col} - 1$, from the bottom one to the top one. By ensuring their order in the vertical direction is

unchanged, the intra-column macro legalization can be solved via dynamic programming (DP):

$$f(i, j) = \min(f(i-1, j - \text{row}(i)) + \text{HPWL}^+(i, j - \text{row}(i) + 1), f(i, j-1)) \quad (4)$$

where $f(i, j)$ represents the increase of HPWL to legalize the 0- i th macros in 0- j th rows of the column, $\text{row}(i)$ represents the number of adjacent rows which should be occupied by macro i , and HPWL^+ denotes the HPWL increase when macro i is placed from row $j - \text{row}(i) + 1$ to row j , compared to the placement before legalization. Variable i will iterate from 0 to $N_{macro,col} - 1$ and Variable j will iterate from 0 to $N_{site,col} - 1$. The intra-column legalization procedures for different columns can be parallelized by assuming that the overall placement of the other parts of the netlist is unchanged.

In AMF-Placer 2.0, when timing effect factor λ in timing-driven quadratic placement illustrated in Section IV-B is greater than a constant hyperparameter $C_{timingLg}$, which is set to 60% empirically, the Eqn.(4) will be replaced by:

$$f(i, j) = \min(f(i-1, j - \text{row}(i)) + \text{Disp}^+(i, j - \text{row}(i) + 1), f(i, j-1)) \quad (5)$$

where Disp^+ denotes the location displacement of macro i when it is placed from row $j - \text{row}(i) + 1$ to row j . Since when timing-slack-based timing terms dominates the timing-driven placement objective function, HPWL turns to be less important while significant displacement of macros might undermine the timing optimized by timing-driven quadratic placement.

Moreover, a new constraint is noticed and considered in AMF-Placer 2.0. Each column of resource on the FPGA device can span multiple clock region but a macro like cascaded DSPs or BRAMs cannot be mapped to sites in different clock regions. Therefore, when calculating $f(i, j)$ for a macro in a column, legality will be verified first and if the checking fails, $f(i, j)$ will be set to an invalid value, e.g., positive infinity. If no valid value is found for macro- $(N_{macro,col} - 1)$, it means no legalization solution for this column and some macros should be moved to the other columns. Therefore, resource supply for this column will be reduced by a given constant ratio, e.g., 5%, and spreading will be conducted again to remove some macros from the column. This procedure will be repeated until all macros are legally mapped to sites.

IV. IMPLEMENTATION OF STA-DEPENDENT PHASES

A. Regression-based Timing Model and Timing Analysis

An accurate timing delay model is a critical component in timing-driven placement.

Previously, Xilinx open-source FPGA EDA framework RapidWright provided a light-weight timing model for Ultrascale-plus devices [45] [46] in a 14/16 nm node, while we target Ultrascale in a 20nm node as most of the previous works due to the license restriction. Generally, it is hard for academic researches to access and handle the numerous low-level information of commercial devices. Moreover, they assumed that two pins on the device will be connected via a known path, which is unknown during placement. Furthermore, it is impractical for us to assume that each pair of pins

are connected via the shortest path in large dense designs. Finally, their provided timing model did not consider the cascaded multi-site macros in practical designs. Other previous works like machine learning-based solution [47] and look-up table-based solutions [29] [48], which are not open-source, rely on the large dataset provided by industry and detailed hyperparameter tuning.

Therefore, AMF-Placer 2.0 includes a regression model for the inter-instance delay (i.e., net delay T_{net}), while a look-up table is used to record the intra-instance delay information (i.e., logic delay, T_{logic}) which are fixed. For the regression model, we first build a dataset of instance-to-instance timing delays of nets in the real-world benchmarks mentioned in Section V-A, which we randomly extract with Vivado Tcl command "get_net_delays". As visualized in Fig. 7, the dataset includes 10000 samples, which are the locations of instances and the routing delay between them determined by the actual routing, and the dataset is provided in our open-source project repository. Then we use a non-integer polynomial function (i.e., polynomial whose degrees could be real number) $T_{net}(e_{i,j})$ to fit the distribution of timing delays with various differences of the X-Y coordinates of interconnected instances on FPGA. The formulation of timing estimation function T is:

$$T_{net}(e_{i,j}) = a_0 \Delta x^{b_0} + a_1 \Delta x^{b_1} + a_2 \Delta y^{b_0} + a_3 \Delta y^{b_1} - Cas(e_{i,j}) + Bkg(x_i, x_j) \quad (6)$$

with $\Delta x = |x_i - x_j|$, $\Delta y = |y_i - y_j|$

where $a_0, a_1, a_2, a_3, b_0, b_1$ are regression factors, x_i, y_i, x_j, y_j are the coordinates of two instances v_i and v_j connected by a timing edge $e_{i,j}$, $Cas(e_{i,j})$ is the delay deduction if $e_{i,j}$ connects two cascaded standard cells in one macro, and $Bkg(x_i, x_j)$ is the extra routing delay when x_i and x_j are in two different available placement regions. $Cas(e_{i,j})$ and $Bkg(x_i, x_j)$ are determined by look-up tables since the related data are regular. A uniform combination of regression factors might not be suitable for various ranges of Δx and Δy because: (1) the samples of net delays are collected from the Vivado placement of real designs where the number of long routing nets is significantly smaller than the number of short routing nets, as shown in Fig. 7; and (2) compared to two distant instances, the routing delay of two close instances are more sensitive to roundabout routing due to the small base value. Therefore, to improve estimation accuracy, timing estimation function T_{net} is separated by several concatenated intervals of $D_{Eucl} = \|(\Delta x, \Delta y)\|$ and among these non-overlap intervals, regression factors could be different, making T a piece-wise function.

In the concrete implementation of AMF-Placer 2.0 targeting Xilinx UltraScale FPGA (xcvu095), T_{net} is separated into 3 intervals of D_{Eucl} , i.e., $[0, 3)$, $[3, 6)$, and $[6, +\infty)$, and meanwhile b_0 and b_1 are found to be 0.3 and 0.5 in the regression model respectively. Accordingly, the fitted regression model is visualized in Fig. 7. As shown in Table. I, where "CPD" represents critical path delay, compared to the Vivado post-route exact critical path delay, the average relative error of our predicted CPD is 8.59% while the average relative error of Vivado pre-route CPD estimation is 7.29%. Our proposed net

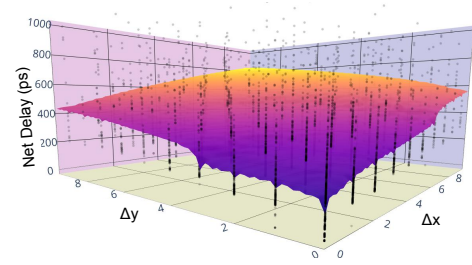


Fig. 7. Dataset Sample Distribution and Regression Model Surface: black markers are samples in our dataset and the surface is generated by the piece-wise function T_{net} with different Δx and Δy

TABLE I
NET DELAY MODEL VALIDATION WITH BENCHMARKS

Benchmark Name	BLSTM	Rosetta DigitRecog	Rosetta FaceDetect	SpoNN	MemN2N	Minimap2	OpenPiton	Average
AMF CPD Prediction (ns)	7.23	9.62	18.37	9.34	9.62	7.61	11.23	-
Relative Error (%)	15.56	8.94	7.35	6.39	9.83	4.43	7.64	8.59
Vivado Pre-Route Prediction CPD (ns)	9.17	12.25	18.59	8.54	12.02	8.19	12.59	-
Relative Error (%)	7.13	16.00	6.25	2.69	12.61	2.93	3.52	7.29
Vivado Post-Route CPD (ns)	8.56	10.56	19.83	8.78	10.67	7.96	12.16	-

delay model is relatively optimistic since most of the samples in the dataset are not in the congested regions while critical paths usually route through congested regions.

Based on the timing model for T_{net} and T_{logic} , and the basic idea of OpenTimer [39], a light-weight parallel static timing analysis (STA) engine is implemented in AMF-Placer 2.0, where the netlist is regarded as a direct acyclic graph with topological levelization and the timing analysis of the instances at the same level will be conducted in parallel. For each instance v_i , the actual arrival time will be:

$$T_{arr}(v_i) = \max_{v_j \in fanin(v_i)} (T_{arr}(v_j) + T_{logic}(v_j) + T_{net}(e_{i,j})) \quad (7)$$

and the required arrival time will be:

$$T_{req}(v_i) = \min_{v_j \in fanout(v_i)} (T_{req}(v_j) - T_{net}(e_{i,j})) - T_{logic}(v_i) \quad (8)$$

Accordingly, similar to [48] [28], for later timing optimization, the slack of a timing edge $e_t(i, j)$ between source instance v_i and sink instance v_j is defined as:

$$Slack(e_t(i, j)) = T_{req}(v_j) - T_{arr}(v_i) - T_{logic}(v_i) - T_{net}(e_{i,j}) \quad (9)$$

and we can get a set of timing edges with negative timing slack $E_t = \{e_t(i, j) | Slack(e_t(i, j)) < 0\}$.

B. Timing-driven Quadratic Placement

As mentioned in Section I-A, analytical placers approximate the wirelength (or HPWL) and some other metrics in numerical models for efficient solutions. Like what many previous analytical placers [6] [8] [9] [43] [38], to approximate the underivable HPWL function,

$$W(\mathbf{x}, \mathbf{y}) = \sum_{e \in E} W_e = \sum_{e \in E} (\max_{i,j \in e} |x_i - x_j| + \max_{i,j \in e} |y_i - y_j|), \quad (10)$$

AMF-Placer use weighted quadratic objective function \widetilde{W}_e , as follows:

$$\widetilde{W}_e = \sum_{i,j \in e} [w_{x,ij}^{B2B} (x_i - x_j)^2 + w_{y,ij}^{B2B} (y_i - y_j)^2], \quad (11)$$

where $w_{x,ij}^{B2B}$ and $w_{y,ij}^{B2B}$ are weights set according to Bound2Bound net model [49]. Then, we can formulate the global placement problem for wirelength minimization as a constrained minimization problem as follows:

$$\begin{aligned} \min_{\mathbf{x}, \mathbf{y}} \quad & \sum_{e \in E} \widetilde{W}_e \\ \text{s.t.} \quad & x_i, y_i \text{ is legal for the type of instance } v_i \end{aligned} \quad (12)$$

Here, a location of an instance is legal when there are enough specific resources for the type of the instance at that location. To make this constrained problem solvable by a quadratic solver, virtual anchors are added to the model. These virtual anchors will be connected to their corresponding instances with artificial two-pin pseudo nets to guide the instances to the legal locations. The wirelength-driven placement problem can transform into one without constraints:

$$\begin{aligned} \min_{\mathbf{x}, \mathbf{y}} \quad & W_{WL}(\mathbf{x}, \mathbf{y}) \\ \text{s.t.} \quad & W_{WL}(\mathbf{x}, \mathbf{y}) = \sum_{e \in E} \widetilde{W}_e + \sum_{e_p \in E_p} [w_{e_p} \widetilde{W}_{e_p}] \end{aligned} \quad (13)$$

where $E_p = \{e_p\}$ is the set of pseudo nets, w_{e_p} is the extra specific weight for pseudo net and \widetilde{W}_{e_p} is the HPWL quadratic approximation of e_p . An example in Fig. 8 shows that an instance could connect to multiple pseudo nets. The greater w_{e_p} is, the more closely the instance can move around from the anchors when solving the quadratic problem.

Compared to [9], [43], [50] and [12], where pseudo nets only connect instances with their locations in last quadratic placement iteration, i.e., the red dash lines in Fig. 8, AMF-Placer 1.0 [33] inserts additional pseudo nets interconnecting instances with their several potential legal locations, which are indicated in Section III-D. Considering macros in the netlist, AMF-Placer 1.0 adds an extra multiplier factor for each pseudo net, which is the number of external pins for the corresponding instance, as shown in Eqn.(14).

$$w_{e_p, v_i} = \alpha / \text{movement}(v_i) \times \text{pinNum}(v_i) \quad (14)$$

With such interconnection-density-aware setting, the macros will be moved slower than the other smaller instances and have heavier gravity toward their potential legal positions, facilitating faster convergence to lower HPWL.

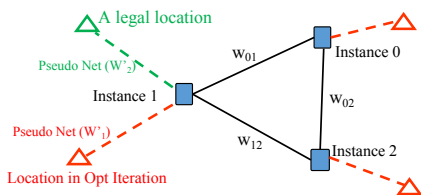


Fig. 8. An Example of Pseudo Nets and Anchors: the dash lines indicate pseudo nets and the triangles represent anchors.

To realize timing-driven placement, timing-aware pin-to-pin pseudo nets should be inserted and the optimization problem of Eqn.(13) is extended to:

$$\begin{aligned} \min_{\mathbf{x}, \mathbf{y}} \quad & (1 - \lambda) W_{WL}(\mathbf{x}, \mathbf{y}) + \lambda W_T(\mathbf{x}, \mathbf{y}) \\ \text{s.t.} \quad & W_{WL}(\mathbf{x}, \mathbf{y}) = \sum_{e \in E} \widetilde{W}_e + \sum_{e_p \in E_p} [w_{e_p} \widetilde{W}_{e_p}] \\ & W_T(\mathbf{x}, \mathbf{y}) = \sum_{e_b \in E_b} [w_{e_b} \widetilde{W}_{e_b}] + \sum_{e_t \in E_t} [w_{e_t} \widetilde{W}_{e_t}] \end{aligned} \quad (15)$$

where E_b is a set of blockage-aware pseudo nets defined in Section III-B, E_t is a set of timing-slack-aware pseudo nets defined in Section IV-A, \widetilde{W}_{e_b} and \widetilde{W}_{e_t} are the HPWL quadratic approximations of e_b and e_t respectively, and λ is a trading-off factor for wirelength and timing which will be gradually increased to realize the smooth transition from wirelength-driven quadratic placement to timing-driven quadratic placement (QP). While the definition of w_{e_b} is provided in Eqn.(1), w_{e_t} is related to $Slack(e_t)$.

Here, we explain the physical meaning of $\sum_{e_t \in E_t} [w_{e_t} \widetilde{W}_{e_t}]$. It can be noticed that since each pseudo net in E_t is a pin-to-pin interconnection, the HPWL approximations of each of them, i.e., \widetilde{W}_{e_t} , is actually the approximations of the Manhattan distances between the pins connected by it [49], which is the first-order approximation of the timing delay. In other words, $\sum_{e_t \in E_t} [w_{e_t} \widetilde{W}_{e_t}]$ can be regarded as a weighted sum of the delays of the timing edges in the timing paths violating the timing constraint. The goal of minimizing this term in Eqn.(15) is to reduce the total negative slack (TNS). However, since the timing edges in E_t could be located in timing paths with different negative slacks, we should assign more weights to the e_t in the most critical timing paths. In previous solutions [29] [48], the criticality of e_t was

$$w_{e_t} = \left(1 - \frac{Slack(e_t)}{Dly_{max}}\right)^{\alpha}$$

where Dly_{max} is the maximum delay in the circuit or a target delay value, and α is the criticality exponent, which can make the weights adaptive to the nets with different criticalities. However, for different applications or at different stages of placement, the timing slack distribution can be various. For example, we notice that some control logic instances or macros with high fanout might be connected to hundreds of instances with tiny negative slacks and several instances with dramatic high negative slacks. The accumulated strength of the tiny negative slacks could prevent the analytical model from resolving the worst negative slack. Moreover, for most scenarios, a relatively small proportion of paths will violate the timing constraints during placement iterations and therefore, it is unnecessary to set timing-aware pin-to-pin nets for all the interconnections in the circuit. Considering these factors, in contrast, in AMF-Placer 2.0, the criticality of e_t is extended as follows:

$$w_{e_t} = \begin{cases} 0 & (Slack(e_t) \geq 0) \\ \left(1 - \frac{Slack(e_t)}{Dly_{max}}\right)^{C(Slack(e_t))} & (Slack(e_t) < 0) \end{cases} \quad (16)$$

with

$$C(\text{Slack}(e_t)) = \max \left(\alpha, \frac{\beta \text{Slack}(e_t)}{T_{thr}} \right) \quad (17)$$

where α and β are parameters to constrain the range of the exponent, and T_{thr} is a negative slack threshold determined by STA which will be called before each quadratic placement iteration. During STA, all the timing edges in the paths with timing violation will be sorted in the ascending order of slack value in a list \mathbf{L}_{NS} and T_{thr} is the threshold to select the top- $\theta\%$ edges in \mathbf{L}_{NS} . T_{thr} is a metric of global timing quality and indicates how WNS is varied from the majority of the slack values of the edges in \mathbf{L}_{NS} . For an edge with negative slack much worse than T_{thr} , w_{e_t} will be aggressively high to resolve the WNS problem. In the actual implementation, α , β and θ are 0.9, 3 and 30 respectively.

Finally, the Eigen3 solver [51] is adopted to handle the optimization for wirelength, TNS and WNS in Eqn.(15), with the high parallelism based on OpenMP.

C. Global Packing

Compared to ASIC placement, during the exact legalization after the FPGA global placement iterations, each instance has to be mapped to sites on the FPGA, each of which consists of fixed number and types of resource. For example, the LUTs, FFs, MUXes and CARRYs with compatible signals can be grouped into on a CLB site to reduce inter-site routing as shown in Fig. 1.

A parallelized packing algorithm with high quality has been proposed by UTPlaceF [38]. It allows the FPGA sites to search their corresponding candidate packing solutions concurrently and then negotiate together during synchronization. AMF-Placer 1.0 has include a set of modifications in this packing solution for higher efficiency. For AMF-Placer 2.0, for timing optimization, timing factor are inserted in the priority evaluation of an instance during parallel packing.

In the site-centric parallel packing algorithm, for each site, the instances with locations close to it will compete to occupy the resources in it. In the original implementation of [38], the priority for instance v_i to occupy the site s_k is formulated as:

$$\text{Priority}_{UTP}(v_i, s_k) = \sum_{e \in \text{Net}(v_i)} \frac{\text{InternalPins}(e, v_i) - 1}{\text{TotalPins}(e) - 1} - \theta \cdot \Delta\text{HPWL}(v_i, s_k) \quad (18)$$

where $\text{Net}(v_i)$ is the set of nets that have at least one cell in s_k , $\text{TotalPins}(e)$ is the total pin count of net e , $\text{InternalPins}(e, v_i)$ is the number of pins of net e in c , and $\Delta\text{HPWL}(v_i, s_k)$ is the HPWL increase of moving instance v_i from their global placement locations (x_i, y_i) to site s_k , θ is a positive weighting parameter. In Eqn.(18), the first term is to reduce the inter-site routing and the second term is to minimize the wirelength overhead. In this procedure, instance v_i might be mapped to a site far away from (x_i, y_i) due to resource contention. After timing-driven global placement, we have obtained a relatively good timing result which we need to preserve during global packing, and therefore, we want those instances on critical paths can be packed into sites close to (x_i, y_i) . We found that

in contrast to the timing slack criticality indicated by Eqn.(9), the longest length of paths including the instance is a better metric during global packing since the placement variation of the instances on the long path will be accumulated to a noticeable downgrading of path delay, which requires high effort during detailed placement to recover. For example, in benchmark FaceDetect [52], there are hundreds of timing paths with more than 50 instances. For one of these paths, given that the clock period constraint is 15ns, the delay of the path after global placement could be around 13ns, and it seems that the timing slack should be flexible for packing. However, if each instance in the path lead to just a tiny timing downgrading, e.g., 0.1ns, the path delay can dramatically increase to more than 18ns, leading to serious timing violation. Accordingly, we include such term in the priority of an instance for a candidate site as follows:

$$\text{Priority}_{AMF} = \text{Priority}_{UTP} + \gamma \sum_{v_i \in V(s_k)} \text{maxPathLen}(v_i) \quad (19)$$

where $\text{maxPathLen}(v_i)$ is the longest length of paths including the instance and γ is a parameter which we set to 0.05 empirically while θ in Priority_{UTP} is set to 0.01.

Apart from the timing optimization, clock legalization is implemented as AMF-Placer 1.0. Additionally, since there are multiple BEL slots in one CLB site as shown in Fig. 1, for the instances mapped to the same CLB site, they will be mapped to the BEL slots by enumerating possible mapping solutions to minimize the timing slacks of the involved timing paths.

D. Detailed Placement

As mentioned in Section IV-B and IV-C, global placement might be dominated by TNS, and global packing might map instances to discrete sites due to resource contention, leading to timing delay increasing of the critical paths. Therefore, to minimize WNS of the placement, detailed placement will be conducted locally for the critical paths while trying to minimize the interference to the other instances. The state-of-the-art solutions for detailed placement are mainly based on the shortest path algorithm [27] [48] [53], which identifies the candidate locations for each node for a timing path under optimization and determines the location for each node to minimize the total delay of the target critical path, as an example shown in Fig. 9 where, A->B->C->D is a target critical path on FPGA, and some candidate locations are identified for each node on this path. For example, instance C can be mapped to site C1, C2, and C3. To formulate the corresponding shortest path problem, a directed acyclic graph

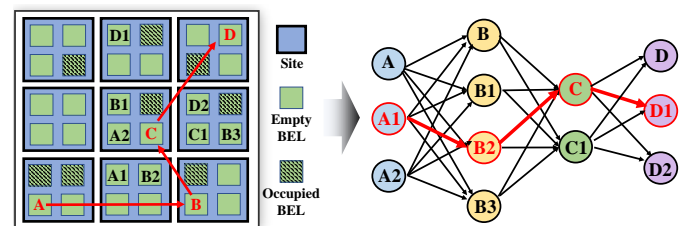


Fig. 9. An example of shortest-path-based detailed placement.

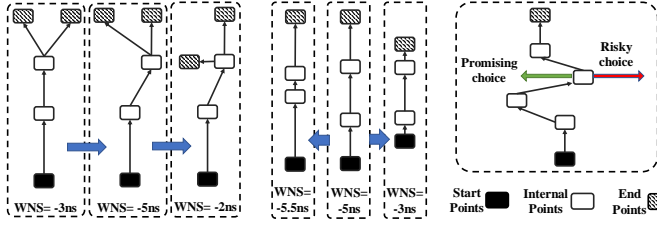


Fig. 10. Examples explaining the motivation of detailed placement strategies

should be constructed with multiple layers, each of which is related to one instance in the critical path and contains vertices corresponding to the candidate sites for the instance. The edge between vertices in different layers represents the corresponding timing delay between two sites for different instances. Accordingly, finding the shortest path from the source layer to the sink layer can map the instances in the path to new sites which can reduce the timing delay of this path.

However, these previous works might suffer from limited timing optimization and high runtime overhead due to two reasons: (1) their solutions subjected to the constraint that no moves or swaps should increase the WNS. However, this constraint might easily trap the placement in local optima and limit the optimization. For example, as shown in Fig. 10, when we reduce the delay of path A by shortest path algorithm, the WNS will get worse as the delay of path B increases, which can be reduced by further optimization iterations to reach a better WNS than the original one; (2) the runtime complexity of the shorted path-based solutions is $O(pL_{avg}N_{candidate}^2)$, where p is a small constant overhead factor [48], L_{avg} is the average length of the critical paths which are considered and $N_{candidate}$ is the average candidate site set size for critical path nodes. Accordingly, a small $N_{candidate}$ will limit the optimization space while a large $N_{candidate}$ will significantly increase the runtime. For example, in [27], $N_{candidate}$ is 25 and if we can reduce it to 10 while preserving the optimization quality, the runtime will be reduced by about 80%.

In contrast, AMF-Placer 2.0 adopts the basic idea of shortest-path-based solution but tolerates temporary increase of WNS during shortest-path-based detailed placement and identifies promising candidates to reduce $N_{candidate}$. The detailed implementation is illustrated as follows.

As shown in Algorithm 1, AMF-Placer 2.0 will go through N_{DPI} iterations. In each iteration of detailed placement, N_{CP} of the critical paths with the highest delay will be extracted as optimization targets via STA and stored in L_{CP} and they will be processed sequentially from the most critical ones to the less critical ones. For a selected target path, conventional shortest path algorithm will be applied and then the instances on the critical path will be marked fixed. These fixed instance cannot be moved by the optimization of the less critical paths in this iteration, and the optimize result for the more critical paths can be preserved. R_{nrb} is a ratio ranging from 1 to 0.1, controlling the maximum distance between the instances and their corresponding candidate sites. In general situations, for each iteration, R_{nrb} will be decreased by ΔR to reduce the number of candidate sites for each instance and N_{CP} will be

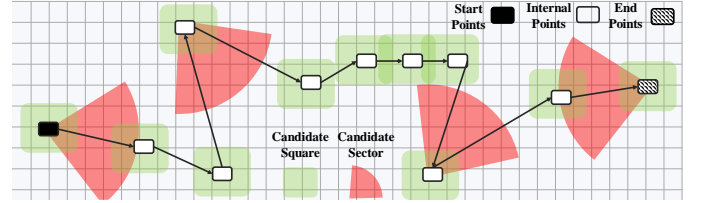


Fig. 11. Examples of sector-based candidate site window

increased by ΔN_{CP} . By controlling R_{nrb} and N_{CP} , at the very beginning of detailed placement, more candidate sites and a smaller number of target critical paths can realize fast improvement of critical path delay (CPD) and WNS, while for the final iterations, less candidate sites and more target critical paths can help to fine-tune the locations of the instances to trade-off the negative slack between overlapped critical paths and further improve TNS by optimizing more paths. The achieved lowest CPD and the corresponding placement will be recorded. If the lowest CPD has not been updated for I_{thr} iterations, the placement will be reset to the recorded best placement, R_{nrb} will be increased by $(I_{thr} + 1)\Delta R$, to provide more improvement potential candidate sites for the most critical paths, and N_{CP} will be reduced by $(I_{thr} + 1)\Delta N_{CP}$ to let the optimization focus on the most critical paths. In an interval of I_{thr} iterations, AMF-Placer 2.0 tolerates the increase of CPD of the circuit. Empirically, N_{DPI} , ΔN_{CP} , ΔR and I_{thr} are set to be 120, 20, 0.01 and 5 respectively.

Algorithm 1: Detailed Placement of AMF-Placer 2.0

Input: netlist information $H = (V, E)$, device information DI , instance locations after global packing $\mathbf{P} = \{(x_i^{pk}, y_i^{pk})\}$
Output: instance locations after optimization $\mathbf{P}' = \{(x_i^{dp}, y_i^{dp})\}$

```

1  $\mathbf{P}' = \mathbf{P}$ 
2  $bestCPD = staticTimingAnalysis(H, DI, \mathbf{P}')$ ;
3  $notOptCnt = 0$ ; // recording the times of optimization failures
4  $N_{CP}, R_{nrb} = 1, 1.0$ ;
5 for  $i=0$ ;  $i < N_{DPI}$ ;  $i++$  do
6    $L_{CP} = getMostCriticalPaths(N_{CP})$ ;
7   foreach  $path \in L_{CP}$  do
8      $candMap = findCandidateLoc(path, \mathbf{P}', DI, R_{nrb})$ ;
9      $\mathbf{P}' = shortestPath(path, candMap, \mathbf{P}')$ ;
10     $markInstancesFixed(path)$ ;
11   $markInstancesUnfixed(L_{CP})$ ;
12   $CPD = staticTimingAnalysis(H, DI, \mathbf{P}')$ ;
13   $R_{nrb} -= \Delta R$ ;  $N_{CP} += \Delta N_{CP}$ ;  $notOptCnt += 1$ ;
14  if  $CPD < bestCPD$  then
15     $bestCPD = CPD$ ;
16     $recordTheBest(\mathbf{P}')$ ;
17     $notOptCnt = 0$ ;
18  else if  $notOptCnt == I_{thr}$  then
19     $recoverToBest(\mathbf{P}')$ ;
20     $notOptCnt = 0$ ;
21     $R_{nrb} += (I_{thr} + 1)\Delta R$ ;
22     $N_{CP} -= (I_{thr} + 1)\Delta N_{CP}$ ;
23  $recoverToBest(\mathbf{P}')$ ;
24  $optPerPathPerSingle_DowngradeNotAllowed(H, DI, \mathbf{P}')$ ;
25 return  $\mathbf{P}'$ 

```

For the concrete optimization of a specific path (i.e., line 8-9 in Algorithm 1), AMF-Placer 2.0 includes a sector-guided candidate selection algorithm which identifies a smaller number of promising candidate sites for path delay optimization. Conventional solutions will select the candidate sites from a $d \times d$ square window around each instance on the path, which might be low-efficiency. According to the examples in Fig. 10, here are our important observations: (1) for the zigzag patterns in a path, a set of beneficial candidate sites for an instance at a turning point with an acute angle in the path can be intuitively identified according to its predecessor and successor in the path; (2) for a smooth or straight path, its overall delay is mainly determined by its start/end points.

Therefore, for candidate identification, AMF-Placer 2.0 uses small $d \times d$ square windows for all the instances on the path, where $d = R_{nbr}R_{Square}$. Meanwhile, additional sector windows, each of which covers a sector of Ω degrees with radius of $r = R_{nbr}R_{Sector}$, will be set for specific instances, which could be the start/end points or internal instances forming an acute triangle with its predecessor and successor. The center of a sector window overlaps with the corresponding instance. For internal instance, the direction of the sector window coincides with the angle bisector of the angle with the instance as its vertex in the triangle constructed with its predecessor and successor. For start/end points, the direction of the sector window coincides with the direction vector from the instance to its successor/predecessor. A concrete example is shown in Fig. 11. It can be noticed that some candidate windows are overlapped and if some BEL slots in these involved CLB sites lead to resource/architecture conflict between instances, the assignment of BEL slots is resolved by balancing the candidate supply among instances, similar to [27]. With such candidate selection algorithm, $N_{candidate}$ in the runtime complexity formula can be significantly reduced. Empirically, R_{Square} , R_{Sector} and Ω are set to be 3, 5 and 90 respectively. In summary, the number of candidate sites for an instance will be determined by both the global timing optimization progress and the local pattern of the instances on critical paths.

At the final stage of detailed placement, the placement update granularity will be transited from the level of multi-path (indicated by N_{CP}) to the level of per-path and per-instance and AMF-Placer 2.0 will enable the constraint of WNS, i.e., no CPD increase will be accepted, to further fine-tune the placement. For these fine-grained updates, an integrated parallel incremental timing analysis is implemented to fast evaluate the timing benefit.

V. EXPERIMENTAL EVALUATION

A. Target Device, Benchmarks and Environment

Currently, AMF-Placer 2.0 mainly targets at Xilinx VU095 FPGA devices but the related techniques can be transferred to other devices. We collect the latest large open-source benchmarks which are open-source, suitable for VU095 device, and designed for various domains, including CNN [54], memory networks [55], LSTM [56], SoC/NoC [57], and genetic encode alignment [34]. The parameters of the benchmarks and device

TABLE II
PARAMETERS OF BENCHMARKS AND DEVICE

Benchmarks	Rosetta [52] FaceDetection	SpoNN [54]	MiniMap2 [60]	OpenPiton [57]	MemN2N [55]	BLSTM [56]	Rosetta [52] DigitRecog	Device: VU095
#LUT	68945	63095	407586	180388	184997	118967	151636	537600
#FF	56987	70987	252624	111966	84694	54690	105580	537600
#CARRY	4978	2091	19826	1712	11528	2762	1970	33600
#Mux	2177	217	180	13696	4466	36210	4662	201600
#LUTRAM	255	251	251	752	3500	1147	251	19200
#DSP	101	165	528	58	312	258	1	768
#BRAM	141	208	283	147	148	812	379	1728
#Cell	134450	137937	681889	309145	289721	215101	265775	-
#Macro	3582	1135	8746	8278	5775	14651	3061	-
#siteForMacro	55666	23079	191263	48066	118960	171822	55754	-
MacroRatio	40%	16%	28%	15%	41%	80%	21%	-
clockPeriod(ns)	15	8%	8	10	10	8	8	-

are listed in Table II, where we use macroRatio, the quotient of the total number of sites required by macros and the total number of sites required by all instances, to indicate the macro proportion of the design. Some of the benchmarks are generated via high-level synthesis [52] while the others are described in Verilog. Some of them contain commercial IP cores. These IP cores are black-box instances in the post-synthesis netlist and cannot be handled by RapidWright [58] and other placers relying on the EDIF (Electronic Design Interchange Format) netlists exported from commercial tools. To overcome this limitation, AMF-Placer 2.0 directly extracts the instance interconnection from Vivado via interactive Tcl commands, to handle general designs. Compared to AMF-Placer 1.0, benchmark OptimSoC [59] is removed since its major cause of timing violation is clock domain crossing (i.e., inter-clock problem). The optimization for multi-clock domain timing is out of the scope of AMF-Placer 2.0. AMF-Placer 2.0 is implemented in C++ and experiments are conducted on Ubuntu 20.04 with Intel i7-6770 CPU (3.40 GHz, 8 logic cores) and 32GB DDR4. All the experiments in this section is run with 8 threads.

B. Comparison with Vivado

Since existing open-source analytical FPGA placers do not support mixed-size FPGA placement of aforementioned macros on Ultrascale devices, for comprehensive comparison, we take the widely-used commercial tool Xilinx Vivado 2020.2 and 2021.2 as our baselines. Specially, Xilinx Vivado 2021.2 is driven by machine learning.

The experimental results are shown in Table III, where WNS represents worst negative slack, CPD represents critical path delay, and RT represents runtime of the entire placement flow. To evaluate the final timing quality, the placement results of AMF-Placer 2.0 will be loaded by Vivado router to implement actual routing, and different combination of placer and router may lead to different results, which is also unveiled in Table III. Here, AMF represents AMF-Placer 2.0, V2020 represents Vivado 2020.2 and V2021 represents Vivado 2021.2. For example, AMF-V2020 represents the combination of AMF-Placer 2.0 and the router of Vivado 2020.1. The WNS metrics indicate how strict the designer-defined timing constraints are, with the consideration of clock skew on the device, and the CPD metrics mainly indicate the delay of the critical path.

TABLE III
COMPARISON OF AMF-PLACER 2.0 WITH VIVADO 2020.2 AND 2021.2

	Place-Route	BLSTM	DigitRecog	FaceDetect	SpoofNN	MemN2N	MiniMap2	OpenPiton	Average
WNS(ns)	AMF-V2020	-0.389	-3.595	-0.384	-0.491	-1.601	0.049	-2.310	-
	AMF-V2021	-0.508	-4.373	-0.445	-0.537	-1.665	0.001	-2.556	-
	V2020	-0.562	-2.564	-0.243	-0.779	-0.669	0.037	-2.159	-
	V2021	-0.668	-3.249	-0.264	-0.836	-0.732	0.070	-2.436	-
CPD(ns)	AMF-V2020	8.40	11.64	15.39	8.50	11.60	7.96	12.32	-
	Rnorm	0.981	1.097	1.009	0.967	1.087	0.999	1.012	1.022
	AMF-V2021	8.51	12.41	15.45	8.55	11.66	8.01	12.56	-
	Rnorm	0.994	1.169	1.013	0.972	1.093	1.006	1.032	1.040
	V2020	8.56	10.61	15.24	8.79	10.67	7.96	12.17	-
	Rnorm	1	1	1	1	1	1	1	1
	V2021	8.67	11.29	15.27	8.85	10.73	7.94	12.44	-
	Rnorm	1.012	1.065	1.002	1.006	1.006	0.996	1.022	1.016
RT(s)	AMF	413	648	292	261	898	1166	679	-
	Rnorm	1.04	1.24	1.02	0.98	1.38	1.07	1.22	1.14
	V2020	398	522	285	265	650	1094	555	-
	Rnorm	1.00	1.00	1.00	1.00	1.00	1.00	1.00	1.00
	V2021	396	529	300	271	759	1031	630	-
	Rnorm	0.99	1.01	1.05	1.02	1.17	0.94	1.14	1.05

According to the table, Vivado 2020.2 realizes the best from the perspectives of both timing quality and runtime. Moreover, the router of Vivado 2020.2 is more suitable for AMF-Placer 2.0. Compared to Vivado 2020.2, AMF-V2020 realizes 2.2% higher CPD and 14% higher runtime on average. Compared to Vivado 2021.2, AMF-V2020 realizes 0.59% higher CPD and 8.5% higher runtime on average.

AMF-Placer 2.0 is the first FPGA placer which can handle the timing-driven mixed-size placement of practical complex designs with various FPGA resources and achieves the comparable quality compared to the latest commercial tools. However, according to the analysis of the concrete placement, we find that the major existing limitations of AMF-Placer 2.0 can be categorized into to three types, listed as follows:

- Timing estimation accuracy: The timing estimation model is relatively optimistic without considering a few of congested regions overlapped with the critical paths, as evaluated in Section IV-A. This problem is noticeable for benchmark DigitRecog [52] and MemN2N [55], which might be resolved by machine-learning-based timing estimation like [47] in the future. Moreover, the timing analysis and optimization at floorplanning stage might be insufficient, which leads to bad start point for the later placement flow and make it extremely hard to reach the optimal placement. Besides, a noticeable proportion of the WNS for benchmark DigitRecog [52] is caused by clock skew, which is not considered by AMF-Placer 2.0 as well as the other existing works for the Ultrascale FPGA architecture. This problem might be resolved according to [61].
- Design-aware factors: The design netlists for Vivado placement are actually hierarchical. According to the placement results of Vivado, based on the design hierarchy information, regularity can be fully utilized for the placement of local circuits, e.g., parallel accumulator datapaths, buses and FIFOs. However, AMF-Pacer 2.0 consumes a flatten netlist, missing the opportunities of regularity-related optimization. This can resolved by reproducing some existing works like [62] and [63].

TABLE IV
EFFECTIVENESS OF PROPOSED OPTIMIZATION TECHNIQUES

	Configuration	BLSTM	DigitRecog	FaceDetect	SpoofNN	MemN2N	MiniMap2	OpenPiton	Average
CPD(ns)	Cfg0	8.40	11.64	15.39	8.50	11.60	7.96	12.32	-
	Rnorm	1	1	1	1	1	1	1	1
	Cfg1	9.31	13.28	16.25	10.18	13.30	8.31	12.72	-
	Rnorm	1.108	1.14	1.056	1.197	1.146	1.044	1.033	1.103
	Cfg2	8.63	13.09	17.73	10.85	12.64	8.44	13.64	-
	Rnorm	1.027	1.125	1.152	1.276	1.09	1.06	1.107	1.120
	Cfg3	8.38	12.46	17.22	11.02	12.36	8.63	12.93	-
	Rnorm	0.997	1.07	1.119	1.297	1.066	1.084	1.05	1.098
	Cfg4	8.40	12.21	15.42	8.65	11.74	7.96	12.67	-
	Rnorm	1.000	1.049	1.002	1.018	1.012	1.001	1.029	1.016
	Cfg5	8.38	12.99	15.39	8.76	11.70	7.96	12.73	-
	Rnorm	0.998	1.116	1	1.03	1.008	1	1.033	1.026
RT(s)	Cfg6	8.39	11.79	15.35	8.68	11.93	7.94	12.90	-
	Rnorm	0.999	1.013	0.997	1.021	1.028	0.997	1.047	1.015
	Cfg0	413	648	292	261	898	1166	679	-
	Rnorm	1	1	1	1	1	1	1	1.00
	Cfg1	393	620	360	229	913	1318	730	-
	Rnorm	0.95	0.96	1.23	0.88	1.02	1.13	1.08	1.04
	Cfg2	431	616	230	227	629	1223	604	-
	Rnorm	1.04	0.95	0.79	0.87	0.7	1.05	0.89	0.90
	Cfg3	419	568	316	232	846	1257	805	-
	Rnorm	1.01	0.88	1.08	0.89	0.94	1.08	1.19	1.01
	Cfg4	432	668	312	279	930	1304	727	-
	Rnorm	1.05	1.03	1.07	1.07	1.04	1.12	1.07	1.06
	Cfg5	466	675	313	274	779	1265	677	-
	Rnorm	1.13	1.04	1.07	1.05	0.87	1.08	1	1.03
	Cfg6	456	661	314	271	896	1288	756	-
	Rnorm	1.10	1.02	1.08	1.04	1.00	1.10	1.11	1.06

C. Effectiveness of Proposed Optimization Techniques

In this subsection, we evaluate the individual impact of the major proposed optimizations for different placement phases in AMF-Placer 2.0. Here we show their impact by setting the placer configurations as follows, to disable different specified optimization technique:

- *Cfg0*: all the optimization techniques are enabled as the configuration in Section V-B.
- *Cfg1*: disable path-length-aware clustering before partitioning in Section III-A
- *Cfg2*: disable blockage-aware spreading and anchor insertion in Section III-B.
- *Cfg3*: disable WNS-aware timing criticality pseudo net weight in Section IV-B, i.e. $C(Slack(e_t)) = \alpha$
- *Cfg4*: disable path-length-aware parallel packing in Section IV-C
- *Cfg5*: disable sector-guided site candidate selection in Section IV-D and the value of R_{Square} remains at 3 (i.e., just using the original small square window)
- *Cfg6*: disable sector-guided site candidate selection in Section IV-D and set R_{Square} to be 5 (i.e., simply enlarge the square window)

According to Table III, we can notice that AMF-Placer 2.0 works better when combined with the router of Vivado 2020.2, and therefore we select "AMF-V2020" for the configurations listed above for comparison.

The experimental results of difference configurations are presented in Table IV. For most of the situations, enabling all the proposed optimization techniques (*Cfg0*) can realize the better timing quality, except for the following two types of cases:

- For benchmark BLSTM [56], disabling WNS-aware timing criticality pseudo net weight (*Cfg3*) can reach a CPD 0.3% lower than *Cfg0* because the timing criticality is distributed evenly in the netlist of BLSTM, making it

benefit less from WNS-aware timing criticality pseudo net weight.

- For benchmark FaceDetect [52], BLSTM [56] and MiniMap2 [60], using a square window large enough for candidate site selection during detailed placement (*Cfg6*) can reach a CPD slightly (0.1%-0.3%) lower than *Cfg0* because these benchmark features a dense placement and the sector-guided candidate window might miss some potential available BEL slots for timing optimization. However, such difference of timing quality is very low for general applications.

It can be noticed that disabling the optimization techniques for global placement (e.g., *Cfg1*, *Cfg2*, and *Cfg3*) can significantly downgrade the timing quality, since the instances can be moved in a wide range and the resultant low-quality placement cannot be compensated by the optimization of detailed placement. Especially, when blockage-aware spreading and anchor insertion are disabled (*Cfg2*), the CPDs of benchmarks increase by 12% on average, indicating the noticeable impact of the placement blockages and the necessity of corresponding optimization.

From the perspective of runtime, disabling the optimization techniques for global placement might reduce the runtime since less analysis and process will be conducted during placement. Especially, disabling blockage-aware spreading and anchor insertion can reduce the runtime by 10% on average for the benchmarks, since currently, the periodically-involved DFS-based clustering is not parallelized and becomes one of the runtime bottlenecks of AMF-Placer 2.0. However considering the benefits of these optimization techniques, these runtime overheads are worthy. It can be noticed that when the path-length-based factor is removed from Eqn.(19) for global packing, the runtime will significantly increase since there are many zigzag critical paths which will cost a lot of runtime for detailed placement to handle them. According to the results of *Cfg5*, using small square windows without sector-windows can also increase the runtime since these narrow windows slow down the optimization progress of the critical paths. The results of *Cfg6* shows that smartly using sector windows for candidate selection during shortest-path-based detailed placement can effectively reduce the runtime while realizing very similar timing quality of the placement obtained with large square windows for candidate selection.

Moreover, in Section IV-D, we have indicated that we

should accept worse CPD temporarily to escape from local optima and reach the optimal CPD of final placement. For example, two traces of CPD of benchmark FaceDetect [52] during the detailed placement are presented in Fig. 12. One of them is the configuration which does not allow downgrading of CPD during detailed placement while the other one is obtained by accepting temporarily timing downgrading. We can find that, although the strict constraint of CPD descending can lead to a smooth CPD optimization trace, tolerating the temporary downgrading can achieve much better final result.

D. Portability to Commercial Tools

A set of toolchains is provided to interact with Vivado like extracting the information of various netlist and device models, which can help users to handle other designs and devices. Placement generated by AMF-Placer can be loaded into Vivado via Tcl script to perform routing. All the placement generated from proposed placement flow in this paper can be successfully routed. However, although timing reports are provided by Vivado, we cannot get the routed wirelength from Vivado because of the license restriction of the Vivado patch in ISPD 2015/2016 contests. Due to limited space, more detailed statistics and usage of AMF-Placer 2.0 are available in the open-source project documentation.

VI. CONCLUSION

In this work, we propose AMF-Placer 2.0, an open-source FPGA placer which can handle the timing-driven mixed-size placement of practical complex designs with various FPGA resources and achieves the comparable quality compared to the latest commercial tools. It is equipped with a series of new techniques for timing optimization, including a simple but effective timing model, placement-blockage-aware anchor insertion, WNS-aware timing-driven quadratic placement, and sector-guided detailed placement. Although limited by the absence of the exact timing model of the device, the information of design hierarchy and accurate routing feedback, experimental results indicate that critical path delays realized by AMF-Placer 2.0 are averagely 2.2% and 0.59% higher than those achieved by commercial tool Xilinx Vivado 2020.2 and 2021.2 respectively. Meanwhile, the average runtime of placement procedure of AMF-Placer 2.0 is 14% and 8.5% higher than Xilinx Vivado 2020.2 and 2021.2 respectively. The source code and Wiki of AMF-Placer, involved open-source benchmarks and the checkpoint/log files for the experiments are available at <https://github.com/zslwyuan/AMF-Placer>.

ACKNOWLEDGMENT

The authors sincerely appreciate the kindly suggestions from reviewers, detailed explanations of UTPlaceF [38] from Dr. Wuxi Li, and useful advice on Vivado metric usages from Dr. Stephen Yang [14], and detailed feedbacks from Mr. Jing Mai, the gold user of AMF-Placer 1.0.

Furthermore, the authors acknowledge support from the Hong Kong Research Grants Council (HK-RGC) General Research Funds (GRF No. 16213521) and thank the anonymous reviewers for their valuable comments to improve the quality of the paper.

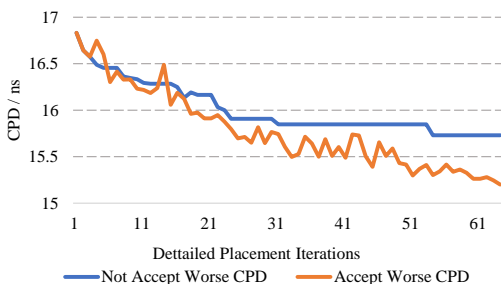


Fig. 12. Example of benchmark FaceDetect [52] shows the benefits of tolerating the temporary downgrading of timing during detailed placement.

REFERENCES

- [1] Xilinx, “Ug974: Ultrascale architecture libraries guide,” 2020.
- [2] C. Lavin, M. Padilla, J. Lamprecht, P. Lundrigan, B. Nelson, and B. Hutchings, “Hmflow: Accelerating fpga compilation with hard macros for rapid prototyping,” in *2011 IEEE 19th Annual International Symposium on Field-Programmable Custom Computing Machines*. IEEE, 2011, pp. 117–124.
- [3] C. M. Fuller, S. W. Gould, S. P. Hartman, E. E. Millham, and G. Yasar, “Field programmable gate arrays using semi-hard multicell macros,” Jun. 2 1998, uS Patent 5,761,078.
- [4] K. E. Murray, O. Petelin, S. Zhong, J. M. Wang, M. Eldafrawy, J.-P. Legault, E. Sha, A. G. Graham, J. Wu, M. J. Walker *et al.*, “Vtr 8: High-performance cad and customizable fpga architecture modelling,” *ACM Transactions on Reconfigurable Technology and Systems (TRETS)*, vol. 13, no. 2, pp. 1–55, 2020.
- [5] G. Chen and J. Cong, “Simultaneous placement with clustering and duplication,” in *Proceedings of the 41st annual Design Automation Conference*, 2004, pp. 740–772.
- [6] M. Gort and J. H. Anderson, “Analytical placement for heterogeneous fpgas,” in *22nd international conference on field programmable logic and applications (FPL)*. IEEE, 2012, pp. 143–150.
- [7] Y.-C. Chen, S.-Y. Chen, and Y.-W. Chang, “Efficient and effective packing and analytical placement for large-scale heterogeneous fpgas,” in *2014 IEEE/ACM International Conference on Computer-Aided Design (ICCAD)*. IEEE, 2014, pp. 647–654.
- [8] W. Li, S. Dhar, and D. Z. Pan, “Utplacef: A routability-driven fpga placer with physical and congestion aware packing,” *IEEE Transactions on Computer-Aided Design of Integrated Circuits and Systems*, vol. 37, no. 4, pp. 869–882, 2017.
- [9] C.-W. Pui, G. Chen, W.-K. Chow, K.-C. Lam, J. Kuang, P. Tu, H. Zhang, E. F. Young, and B. Yu, “Ripplefpga: A routability-driven placement for large-scale heterogeneous fpgas,” in *2016 IEEE/ACM International Conference on Computer-Aided Design (ICCAD)*. IEEE, 2016, pp. 1–8.
- [10] R. Pattison, Z. Abuowaimer, S. Areibi, G. Gréwal, and A. Vannelli, “Gplace: A congestion-aware placement tool for ultrascale fpgas,” in *2016 IEEE/ACM International Conference on Computer-Aided Design (ICCAD)*. IEEE, 2016, pp. 1–7.
- [11] Y.-C. Kuo, C.-C. Huang, S.-C. Chen, C.-H. Chiang, Y.-W. Chang, and S.-Y. Kuo, “Clock-aware placement for large-scale heterogeneous fpgas,” in *2017 IEEE/ACM International Conference on Computer-Aided Design (ICCAD)*. IEEE, 2017, pp. 519–526.
- [12] D. Vercruyce, E. Vansteenkiste, and D. Stroobandt, “Liquid: High quality scalable placement for large heterogeneous fpgas,” in *2017 International Conference on Field Programmable Technology (ICFPT)*, 2017, pp. 17–24.
- [13] W. Li, Y. Lin, and D. Z. Pan, “elfplace: Electrostatics-based placement for large-scale heterogeneous fpgas,” in *2019 IEEE/ACM International Conference on Computer-Aided Design (ICCAD)*. IEEE, 2019, pp. 1–8.
- [14] S. Yang, A. Gayasen, C. Mulpuri, S. Reddy, and R. Aggarwal, “Routability-driven fpga placement contest,” in *Proceedings of the 2016 on International Symposium on Physical Design*, 2016, pp. 139–143.
- [15] S. Yang, C. Mulpuri, S. Reddy, M. Kalase, S. Dasasathyan, M. E. Dehkordi, M. Tom, and R. Aggarwal, “Clock-aware fpga placement contest,” in *Proceedings of the 2017 ACM on International Symposium on Physical Design*, 2017, pp. 159–164.
- [16] P. Liao, S. Liu, Z. Chen, W. Lv, Y. Lin, and B. Yu, “Dreamplace 4.0: timing-driven global placement with momentum-based net weighting,” in *2022 Design, Automation & Test in Europe Conference & Exhibition (DATE)*. IEEE, 2022, pp. 939–944.
- [17] D. Hyun, Y. Fan, and Y. Shin, “Accurate wirelength prediction for placement-aware synthesis through machine learning,” in *2019 Design, Automation & Test in Europe Conference & Exhibition (DATE)*. IEEE, 2019, pp. 324–327.
- [18] N. Viswanathan, G.-J. Nam, J. A. Roy, Z. Li, C. J. Alpert, S. Ramji, and C. Chu, “Itop: Integrating timing optimization within placement,” in *Proceedings of the 19th International Symposium on Physical Design*, ser. ISPD ’10. New York, NY, USA: Association for Computing Machinery, 2010, p. 83–90. [Online]. Available: <https://doi.org/10.1145/1735023.1735048>
- [19] A. Bock, S. Held, N. Kämmerling, and U. Schorr, “Local search algorithms for timing-driven placement under arbitrary delay models,” in *Proceedings of the 52nd Annual Design Automation Conference*, ser. DAC ’15. New York, NY, USA: Association for Computing Machinery, 2015. [Online]. Available: <https://doi.org/10.1145/2744769.2744867>
- [20] V. Livramento, R. Netto, C. Guth, J. L. Güntzel, and L. C. V. D. Santos, “Clock-tree-aware incremental timing-driven placement,” *ACM Trans. Des. Autom. Electron. Syst.*, vol. 21, no. 3, apr 2016. [Online]. Available: <https://doi.org/10.1145/2858793>
- [21] G. Wu and C. Chu, “Two approaches for timing-driven placement by lagrangian relaxation,” *IEEE Transactions on Computer-Aided Design of Integrated Circuits and Systems*, vol. 36, no. 12, pp. 2093–2105, 2017.
- [22] T. Ajayi, V. A. Chhabria, M. Fogaça, S. Hashemi, A. Hosny, A. B. Kahng, M. Kim, J. Lee, U. Mallappa, M. Neseem *et al.*, “Toward an open-source digital flow: First learnings from the openroad project,” in *Proceedings of the 56th Annual Design Automation Conference 2019*, 2019, pp. 1–4.
- [23] D. Mangiras, A. Stefanidis, I. Seitanidis, C. Nicopoulos, and G. Dimitrakopoulos, “Timing-driven placement optimization facilitated by timing-compatibility flip-flop clustering,” *IEEE Transactions on Computer-Aided Design of Integrated Circuits and Systems*, vol. 39, no. 10, pp. 2835–2848, 2020.
- [24] Y.-C. Lu, S. Pentapati, and S. K. Lim, “The law of attraction: Affinity-aware placement optimization using graph neural networks,” in *Proceedings of the 2021 International Symposium on Physical Design*, 2021, pp. 7–14.
- [25] B. N. Trombley, N. D. Hieter, and D. A. Gay, “Path-based timing driven placement using iterative pseudo netlist changes,” Mar. 29 2022, uS Patent 11,288,425.
- [26] S.-Y. Chen and Y.-W. Chang, “Routing-architecture-aware analytical placement for heterogeneous fpgas,” in *2015 52nd ACM/EDAC/IEEE Design Automation Conference (DAC)*, 2015, pp. 1–6.
- [27] S. Dhar, M. A. Iyer, S. Adya, L. Singhal, N. Rubanov, and D. Z. Pan, “An effective timing-driven detailed placement algorithm for fpgas,” in *Proceedings of the 2017 ACM on International Symposium on Physical Design*, 2017, pp. 151–157.
- [28] Z. Lin, Y. Xie, G. Qian, S. Wang, J. Yu, and J. Chen, “An analytical timing-driven placer for heterogeneous fpgas: late breaking results,” in *Proceedings of the 57th ACM/EDAC/IEEE Design Automation Conference*, 2020, pp. 1–2.
- [29] Z. Lin, Y. Xie, G. Qian, J. Chen, S. Wang, J. Yu, and Y.-W. Chang, “Timing-driven placement for fpgas with heterogeneous architectures and clock constraints,” in *2021 Design, Automation & Test in Europe Conference & Exhibition (DATE)*. IEEE, 2021, pp. 1564–1569.
- [30] S. Nikolić, G. Zgheib, and P. Ienne, “Detailed placement for dedicated lut-level fpga interconnect,” *ACM Trans. Reconfigurable Technol. Syst.*, nov 2021, just Accepted. [Online]. Available: <https://doi.org/10.1145/3501802>
- [31] D. Stroobandt, J. Depreitere, and J. Van Campenhout, “Generating new benchmark designs using a multi-terminal net model,” *Integration*, vol. 27, no. 2, pp. 113–129, 1999.
- [32] J. Mai, Y. Meng, Z. Di, and Y. Lin, “Multi-electrostatic fpga placement considering slicel-slicem heterogeneity and clock feasibility,” 2022.
- [33] T. Liang, G. Chen, J. Zhao, S. Sinha, and W. Zhang, “Amf-placer: High-performance analytical mixed-size placer for fpga,” in *2021 IEEE/ACM International Conference On Computer Aided Design (ICCAD)*. IEEE, 2021, pp. 1–9.
- [34] L. Guo, J. Lau, Z. Ruan, P. Wei, and J. Cong, “Hardware acceleration of long read pairwise overlapping in genome sequencing: A race between fpga and gpu,” in *2019 IEEE 27th Annual International Symposium on Field-Programmable Custom Computing Machines (FCCM)*. IEEE, 2019, pp. 127–135.
- [35] Xilinx, “Ug574: Ultrascale architecture configurable logic block,” 2017.
- [36] —, “Ug573: Ultrascale architecture memory resources,” 2021.
- [37] —, “Ug579: Ultrascale architecture dsp slice,” 2020.
- [38] W. Li and D. Z. Pan, “A new paradigm for fpga placement without explicit packing,” *IEEE Transactions on Computer-Aided Design of Integrated Circuits and Systems*, vol. 38, no. 11, pp. 2113–2126, 2018.
- [39] T.-W. Huang and M. D. Wong, “Opentimer: A high-performance timing analysis tool,” in *2015 IEEE/ACM International Conference on Computer-Aided Design (ICCAD)*. IEEE, 2015, pp. 895–902.
- [40] Ü. V. Çatalyürek and C. Aykanat, “Patoh (partitioning tool for hypergraphs),” in *Encyclopedia of Parallel Computing*. Springer, 2011, pp. 1479–1487.
- [41] J. Chen, Z. Lin, Y.-C. Kuo, C.-C. Huang, Y.-W. Chang, S.-C. Chen, C.-H. Chiang, and S.-Y. Kuo, “Clock-aware placement for large-scale heterogeneous fpgas,” *IEEE Transactions on Computer-Aided Design of Integrated Circuits and Systems*, vol. 39, no. 12, pp. 5042–5055, 2020.
- [42] T. Heuer, “High quality hypergraph partitioning via max-flow-min-cut computations,” Ph.D. dissertation, Master’s thesis, KIT, 2018.

- [43] M.-C. Kim, D.-J. Lee, and I. L. Markov, “Simpl: An effective placement algorithm,” *IEEE Transactions on Computer-Aided Design of Integrated Circuits and Systems*, vol. 31, no. 1, pp. 50–60, 2011.
- [44] T. Lin, C. Chu, and G. Wu, “Polar 3.0: An ultrafast global placement engine,” in *2015 IEEE/ACM International Conference on Computer-Aided Design (ICCAD)*, 2015, pp. 520–527.
- [45] P. Maidee, C. Neely, A. Kaviani, and C. Lavin, “An open-source lightweight timing model for rapidwright,” in *2019 International Conference on Field-Programmable Technology (ICFPT)*. IEEE, 2019, pp. 171–178.
- [46] Y. Zhou, P. Maidee, C. Lavin, A. Kaviani, and D. Stroobandt, “Rwroute: An open-source timing-driven router for commercial fpgas,” *ACM Trans. Reconfigurable Technol. Syst.*, vol. 15, no. 1, nov 2021. [Online]. Available: <https://doi.org/10.1145/3491236>
- [47] T. Martin, G. Grewal, and S. Areibi, “A machine learning approach to predict timing delays during fpga placement,” in *2021 IEEE International Parallel and Distributed Processing Symposium Workshops (IPDPSW)*, 2021, pp. 124–127.
- [48] T. Martin, D. Maarouf, Z. Abuowaimer, A. Alhyari, G. Grewal, and S. Areibi, “A flat timing-driven placement flow for modern fpgas,” in *Proceedings of the 56th Annual Design Automation Conference 2019*, 2019, pp. 1–6.
- [49] P. Spindler, U. Schlichtmann, and F. M. Johannes, “Kraftwerk2—a fast force-directed quadratic placement approach using an accurate net model,” *IEEE Transactions on Computer-Aided Design of Integrated Circuits and Systems*, vol. 27, no. 8, pp. 1398–1411, 2008.
- [50] T. Lin and C. Chu, “Polar 2.0: An effective routability-driven placer,” in *Proceedings of the 51st Annual Design Automation Conference*, 2014, pp. 1–6.
- [51] G. Guennebaud, B. Jacob *et al.*, “The eigen 3 c++ library,” 2010.
- [52] Y. Zhou, U. Gupta, S. Dai, R. Zhao, N. Srivastava, H. Jin, J. Featherston, Y.-H. Lai, G. Liu, G. A. Velasquez *et al.*, “Rosetta: A realistic high-level synthesis benchmark suite for software programmable fpgas,” in *Proceedings of the 2018 ACM/SIGDA International Symposium on Field-Programmable Gate Arrays*, 2018, pp. 269–278.
- [53] Z. Lin, Y. Xie, P. Zou, S. Wang, J. Yu, and J. Chen, “An incremental placement flow for advanced fpgas with timing awareness,” *IEEE Transactions on Computer-Aided Design of Integrated Circuits and Systems*, vol. 41, no. 9, pp. 3092–3103, 2022.
- [54] K. Kara, “Spoonnn: Fpga-based neural network inference library,” 2018.
- [55] S. Sukhbaatar, A. Szlam, J. Weston, and R. Fergus, “End-to-end memory networks,” *arXiv preprint arXiv:1503.08895*, 2015.
- [56] V. Rybalkin, N. Wehn, M. R. Yousefi, and D. Stricker, “Hardware architecture of bidirectional long short-term memory neural network for optical character recognition,” in *Design, Automation & Test in Europe Conference & Exhibition (DATE)*, 2017. IEEE, 2017, pp. 1390–1395.
- [57] J. Balkind, M. McKeown, Y. Fu, T. Nguyen, Y. Zhou, A. Lavrov, M. Shahrad, A. Fuchs, S. Payne, X. Liang *et al.*, “Openpiton: An open source manycore research framework,” *ACM SIGPLAN Notices*, vol. 51, no. 4, pp. 217–232, 2016.
- [58] C. Lavin and A. Kaviani, “Rapidwright: Enabling custom crafted implementations for fpgas,” in *2018 IEEE 26th Annual International Symposium on Field-Programmable Custom Computing Machines (FCCM)*. IEEE, 2018, pp. 133–140.
- [59] S. Wallentowitz, P. Wagner, M. Tempelmeier, T. Wild, and A. Herkersdorf, “Open tiled manycore system-on-chip,” *arXiv preprint arXiv:1304.5081*, 2013.
- [60] L. Guo, J. Lau, Z. Ruan, P. Wei, and J. Cong, “Hardware acceleration of long read pairwise overlapping in genome sequencing: A race between fpga and gpu,” in *2019 IEEE 27th Annual International Symposium on Field-Programmable Custom Computing Machines (FCCM)*. IEEE, 2019, pp. 127–135.
- [61] K. Zhu and D. Wong, “Clock skew minimization during fpga placement,” in *Proceedings of the 31st annual Design Automation Conference*, 1994, pp. 232–237.
- [62] J.-M. Lin, W.-F. Huang, Y.-C. Chen, Y.-T. Wang, and P.-W. Wang, “Dapa: A dataflow-aware analytical placement algorithm for modern mixed-size circuit designs,” in *2021 IEEE/ACM International Conference On Computer Aided Design (ICCAD)*, 2021, pp. 1–8.
- [63] D. Fang, B. Zhang, H. Hu, W. Li, B. Yuan, and J. Hu, “Global placement exploiting soft 2d regularity,” in *Proceedings of the 2022 International Symposium on Physical Design*, ser. ISPD ’22. New York, NY, USA: Association for Computing Machinery, 2022, p. 203–210. [Online]. Available: <https://doi.org/10.1145/3505170.3506723>